International Journal of Impact Engineering 93 (2016) 196–210

Contents lists available at ScienceDirect

International Journal of Impact Engineering

journal homepage: www.elsevier.com/locate/ijimpeng

# Compressive response of sandwich plates to water-based impulsive loading

Siddharth Avachat, Min Zhou *

*The George W. Woodruff School of Mechanical Engineering, School of Materials Science and Engineering, Georgia Institute of Technology, Atlanta, GA 30332-0405, USA*

ARTICLE INFO

*Article history:*
Received 17 December 2014
Received in revised form 5 March 2016
Accepted 8 March 2016
Available online 14 March 2016

*Keywords:*
Underwater blast loading
Fluid structure interaction (FSI) and multiphysics
Sandwich structures
Structural polymeric foams
Dynamic deformation and failure

ABSTRACT

The compressive response of sandwich plates with polyvinyl chloride (PVC) foam cores and aluminum facesheets to water-based impulsive loading is analyzed using an instrumented impulsive loading apparatus called the underwater shock loading simulator (USLS) and a fully-dynamic 3-D computational framework. The loading conditions analyzed are similar to those in underwater blasts. The study focuses on the overall deformation, strain recovery and impulse transmission which are quantified as functions of structural attributes such as core density, front and backface masses, and incident impulsive load intensity. Measurements obtained using high-speed digital imaging and pressure and force sensors allow the computational models to be calibrated and verified. Quantitative loading–structure–performance maps are developed between the response variables and structural and load attributes. The results reveal that core density has the most pronounced influence on core compressive strain and impulse transmission. Specifically, for severe impulse intensities, a 100% increase in core density leads to a 200% decrease in compressive strain and a 500% increase in normalized transmitted impulse. On the other hand, structures with low density cores are susceptible to collapse at high impulse intensities. Additionally, the compressive strains and transmitted impulses increase monotonically as the mass of the frontface increases, but are unaffected by backface mass. For the same core density, a 100% increase in facesheet thickness leads to a 25% and 50% increase in the core strain and normalized transmitted impulse, respectively. The results and performance maps are useful for designing marine structures with restricts, such as hull sections and pipelines backed by water or machinery.



## 1. Introduction

Marine vessels operate in severe environments with temperature extremes, transient loads and corrosive sea water. In addition to operational loads, the structures are required to withstand accidental hydrodynamic impulsive loads due to surface and sub-surface blasts and weapons impact. Sandwich composites can provide good blast mitigation due to their high strength-to-weight ratios and high shear and bending resistances. Previous research on the dynamic behavior of sandwich composites has focused on low velocity, contact-based loads such as drop weight and projectile impact [1–8]. It is found that the overall deflection experienced by sandwich plates is significantly lower than monolithic plates of equivalent mass. Additionally, the forces and impulses transmitted by sandwich structures are significantly smaller than those transmitted by monolithic structures [9–11]. Recent assessments of blast-loaded marine structures show that fluid structure interaction (FSI) effects play an important role in response and can be exploited to improve the blast mitigation capability [12–21]. The deformation and failure of sandwich structures subjected to underwater impulsive loads are complicated due to competing damage mechanisms, complex failure modes, interfacial effects and material heterogeneity. The facesheets have a dominant effect on the rigidity of the sandwich structure and provide protection from environmental conditions while the core governs the energy absorption by, and impulse transmission, through the structure. In addition, load intensities, boundary conditions, and operating environments all influence deformation and failure. Despite recent advances in understanding, several key issues remain unresolved.

The objective of the present combined experimental and numerical study is to characterize the behavior of structural foams subjected to underwater impulsive loads and delineate the role of core compressibility and facesheet thickness on the response of sandwich plates. The focus is on quantifying the compression and impulse transmission characteristics of PVC foams with a range of densities under loading of water-based, high-intensity impulses generated using a recently developed experimental setup called the underwater shock loading simulator (USLS). The loads mimic the high-pressure, exponentially-decaying impulses that are generated during

* Corresponding author. The George W. Woodruff School of Mechanical Engineering, School of Materials Science and Engineering, Georgia Institute of Technology, Atlanta, GA 30332-0405, USA. Tel.: +404 894 3294; Fax: +404 894 0186.
*E-mail address:* min.zhou@gatech.edu (M. Zhou).

http://dx.doi.org/10.1016/j.ijimpeng.2016.03.007
0734-743X/

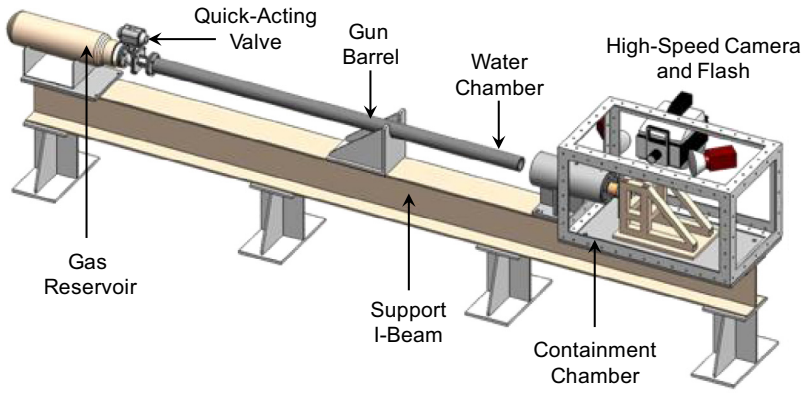


**Fig. 1.** A schematic illustration of the underwater shock loading simulator (USLS) and a photograph of the facility.

underwater explosions. As shown in Fig. 1, the USLS consists of a projectile-impact-based impulsive loading system, a water chamber, a target holder and a safety enclosure. In-situ measurements of the material response are obtained using high-speed digital imaging and force transducers, providing an opportunity to assess the role of core density and strength on blast resistance during events mimicking an underwater detonation.

## 2. Instrumented underwater impulsive loading apparatus

Gas gun impact has been successfully used to generate impulsive loading through water [12–15,22]. To obtain controlled loading and simulate different water-structure contact conditions, the underwater shock loading simulator (USLS) in Fig. 1 is designed to provide a variety of load configurations with quantitative diagnostics [12,13,22]. Important features of this facility include the ability to generate water-based impulsive loading of a wide range of intensity, the ability to simulate the loading of submerged structures, and integrated high-speed photographic and laser interferometric diagnostics. Fig. 2 shows a schematic illustration of the cross-section of the USLS.

The shock tube is an 800 mm long cylinder which is horizontally mounted and filled with water. It is made of steel and has an inside diameter of 80 mm. A thin piston plate is mounted at the front end and the specimen is located at the rear end. A projectile is accelerated by the gas gun and strikes the piston plate, generating a planar pressure pulse in the shock tube. The impulsive load that impinges on the target induces deformation in the specimen at strain rates up to $10^4\ s^{-1}$. Projectile impact velocities in the range of 15–150 $ms^{-1}$ are used to delineate the effect of loading rate on the deformation and failure behavior of the structures analyzed. This velocity range corresponds to peak pressures between 15 and 200 MPa, which are comparable to pressures observed in underwater explosions [16–18]. The metal platens have a thickness of 10 mm and a diameter of 100 mm; while the foam specimens have a thickness of 50 mm and a diameter of 70 mm.

The uniaxial compressive loading setup developed for this analysis is referred to as the "Dynacomp" setup. Here, an aluminum platen is held in contact with water on one side of the platen and a deformable core on the opposite side of the platen. This deformable core is supported by another aluminum platen which rests on a force transducer embedded in a 25 mm thick steel plate. A flange is designed to ensure that the foam core is always in contact with the aluminum platens on both the impulse side and the opposite side and is held normal to the platens. Care is taken to ensure that there is no slippage between the platens and the core. The compressive strain of the foam core is obtained via high-speed digital imaging and the transmitted impulse is measured using a high dynamic range force transducer. These two parameters provide a description of the compressive response and help quantify the blast mitigation capability of each core configuration. Additionally, the front and backface thicknesses can be varied to evaluate the effect of both variables on the foam core.

According to Taylor's analysis of one dimensional blast waves [19] impinging on a light, rigid, free standing plate, the pressure in the fluid at a distance $r$ from an explosive source follows the relation $p(t) = p_0 \exp(-t/t_0)$, where $p_0$ is the peak pressure, $t$ is time and $t_0$ is the pulse time on the order of milliseconds. The area under the pressure–time curve is the impulse carried by

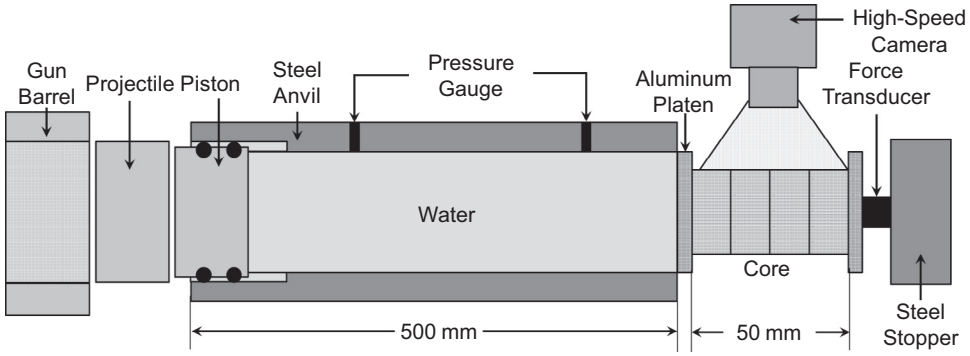


**Fig. 2.** A schematic illustration of the dynamic compression "Dynacomp" test setup within the underwater shock loading simulator (USLS).

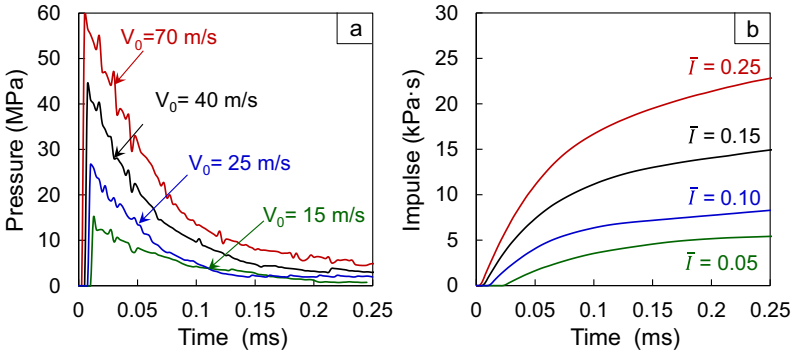


**Fig. 3.** (a) The pressure profiles of impulsive waves in the water chamber measured in experiments for four different projectile velocities; (b) the corresponding normalized incident impulses $(\bar{I})$.

the wave and is given by $I_0 = \int_0^t p(t)dt = p_0 t_0$. For a free standing plate of areal mass $m$, the impulse transferred to the plate is $I_T/I_0 = \psi^{(\psi/1-\psi)}$, where $\psi = \rho_w c_w t_0/m$ and $\rho_w$ is the density of water and $c_w$ is the speed of sound in water. This FSI parameter is an important aspect of Taylor's analysis because it helps to delineate the effects of a pressure pulse applied instantaneously versus the effects of a pressure pulse decaying over a certain time period. It has been shown that this FSI effect can be exploited to improve the blast mitigation capability of structures subjected to transient loads [20,21]. It can be deduced that the impulse transferred to a plate is highly dependent on the mass of that plate. An incoming wave will transfer a very small impulse to a light plate supported by a core with very low strength. Conversely, if the core is strong and resistant to deformation, a larger impulse is transferred to the structure than that predicted by Taylor's analysis. For the upper limit, i.e., an infinitely heavy plate subjected to an intense shock, the entire incident impulse is transferred to the plate. For the loading configuration considered here, the frontface is supported by a core and backface. The backface is fitted with a force transducer and the entire assembly is prevented from moving by a heavy steel plate. Hutchinson and Xue [8] provided a correction to account for a "pushback" effect when the frontface of areal mass $m_f$ resists motion by virtue of being supported by a core with compressive yield strength $\sigma_Y^c$ such that

$$\bar{I}_T = I_T/I_0 = \psi^{(\psi/1-\psi)} + 0.63\sigma_Y^c/p_0\left(1-\psi^{(\psi/1-\psi)}\right), \quad (1)$$

and the momentum/area transferred to the core and backface being

$$\bar{I}_B = I_B/I_0 = 1.82\sigma_Y^c/p_0\left(1-\psi^{(\psi/1-\psi)}\right). \quad (2)$$

The impulse acquired by the frontface of a sandwich structure is $\bar{I}_F = I_F/I_0 = I_T/I_0 - I_B/I_0$. It should be noted that Xue and Hutchinson's work is applicable to relatively weak, perfectly plastic cores that provide a uniform stress-saturated compressive strain response. Additionally, Taylor's $I_T/I_0$ relation is independent of impulsive load intensity while Hutchinson and Xue's $I_T/I_0$ relation is dependent on the peak pressure of the incident impulse as well as the yield strength of the core, leading to a loss in generality. In the Dynacomp setup, the backface is essentially immovable and the force transducers fitted to the backface enable the calculation of impulse transmitted through the thickness of the sandwich plate. The reaction force histories can be converted to impulses transmitted via $I_B = \int F \cdot dt/A$, where $F$ is the reaction force and $A$ is the area under loading. A normalized transmitted impulse is then expressed as $\bar{I}_B = I_B/I_0$. The transmitted impulse $\bar{I}_B$ is an important metric to evaluate the blast mitigation capability of a sandwich structure. It can be inferred from Eqn. (2) that a lower value of $I_B/I_0$ for a specific incident pressure pulse corresponds to better blast mitigation capability of a particular core and the higher the FSI parameter.

For the current analysis, the non-dimensionalized incident impulse $\bar{I}$ in the form of $\bar{I} = I_0/\rho_w c_w\sqrt{A}$ is used, where $A$ is the area of loading. Pressures ranging from 10 MPa to 100 MPa can be generated using different projectile velocities. Fig. 3 shows experimentally measured pressure histories and corresponding impulses for four different projectile velocities. A comparison of experimentally measured and numerically calculated pressure pulses corresponding to a projectile velocity of 70 ms$^{-1}$ is provided in Fig. 4. The rise time of the pressure pulses is on the order of 25 μs and the decay time is on the order of 250 μs. The impulsive loads have peak pressures of 18, 28, 43, 59 MPa which approximately correspond to 100 kg of TNT detonating at distances of 12, 8, 5.5 and 4.2 meters, respectively, based on the relationship proposed by Swisdak [16].

## 3. Underwater impulsive loading experiments

The materials analyzed are structural poly-vinyl chloride (PVC) foams manufactured by DIAB Inc. [23] under the trade name Divinycell HP. These foams are used because their high residual strengths and dimensional stability make them ideal for vacuum bagging and vacuum assisted resin-transfer molding (VARTM). The high strength-to-weight ratio of sandwich structures manufactured using these foams lead to higher vehicle speeds, greater payload capacities, and reduced power demand, all of which result in better operating economy. Additionally, these structural foams possess high chemical resistance, low water absorbency and good thermal insulation and make ideal core materials in sandwich constructions for marine applications. Here, PVC foams with densities of 60, 100, 130, 200 and 250 kg/m$^3$ are studied. The height of the specimen ($T_c$) is 50 mm and the diameter ($D$) is 75 mm. The total thickness of the specimen is $T = T_c + T_f + T_b$ where $T_c, T_f$ and $T_b$ are the core, frontface and backface thicknesses, respectively. The compressive stress–strain responses for the core materials, as obtained by George et al. [24], are shown in Fig. 5. The stress–strain relations are linear initially and subsequently show yielding and stress saturation before core densification which leads to a rise in stress. This unique characteristic of the compressive deformation makes the foams especially useful for applications requiring compression and energy absorbency. To compare the effects of different core densities, a normalized density in the form of $\bar{\rho} = \rho_{core}/\rho_{face}$ is used, where $\rho_{core}$ is the density of the foam and $\rho_{face}$ is the density of the facesheet material (aluminum).

The circular platens are machined from 12 mm thick 6061 aluminum alloy plates which have a yield strength of 275 MPa and density of 2700 kg m$^{-3}$. This strength is adequate to ensure that the

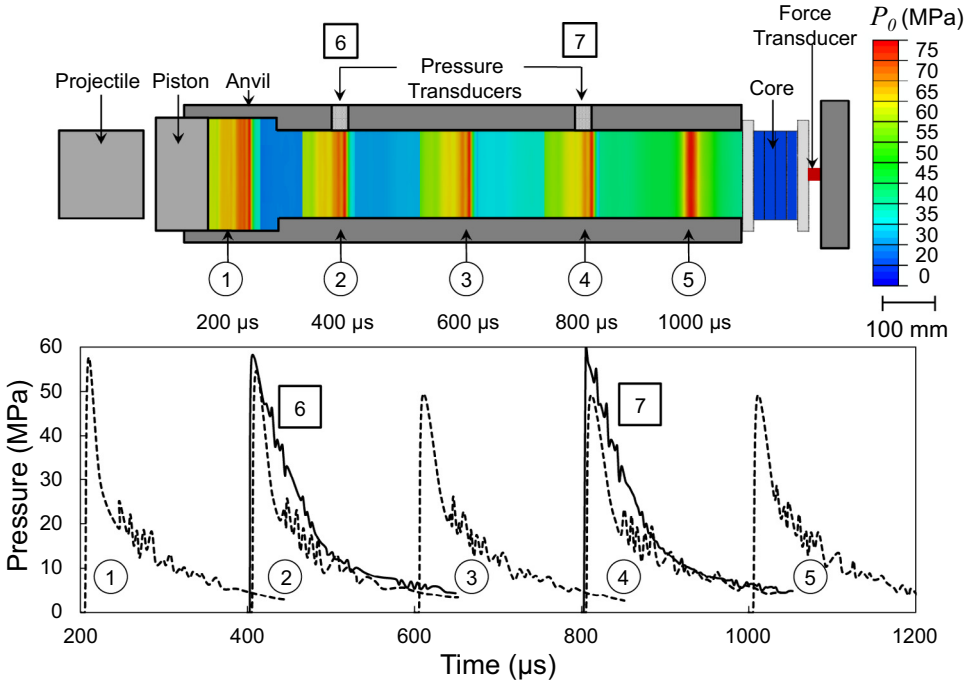


**Fig. 4.** Cross-sectional view of the *Dynacomp* setup showing the distributions of experimentally measured (square-boxed numbers) and numerically calculated (circled numbers) pressure distributions at different locations for an impulsive wave generated with a projectile velocity of 70 $ms^{-1}$ ( $\bar{I} = 0.25$).

platens undergo negligible plastic deformation under the impulsive loads considered. In the initial set of experiments, the front and backface thicknesses are $T_f = T_b = 12$ mm. To evaluate the effect of frontface mass on the overall response, the thicknesses are increased gradually. The normalized front and backface thicknesses are non-dimensionalized as $T_f/T_c$ and $T_b/T_c$, respectively, where $T_c$ is the core thickness. The facesheet thicknesses are increased gradually and the changes are denoted by $\Delta T_f$ and $\Delta T_b$, respectively. The values for $\Delta T_f$ and $\Delta T_b$ are 4, 6, 8 and 10 mm, giving face thickness-to-core thickness ratios $(\Delta T_f/T_c)$ and $(\Delta T_b/T_c)$ of 0.08, 0.12, 0.16 and 0.2. The densities of the platens and the facesheets are much higher than those of the foam cores, so the platens can be considered as effectively rigid.

## 4. Numerical model

The numerical calculations are carried out using the commercial finite element code Abaqus/Explicit [25]. The Mie–Grüneisen equation of state is used to simulate the behavior of water, and the modified Drucker Prager constitutive model developed by Deshpande and Fleck [26] coupled with the damage criterion proposed by Hooputra et al. [27] is used to capture the deformation and fracture in Divinycell HP PVC structural foams. The elements used in this analysis are 3-D 8-noded linear brick elements.

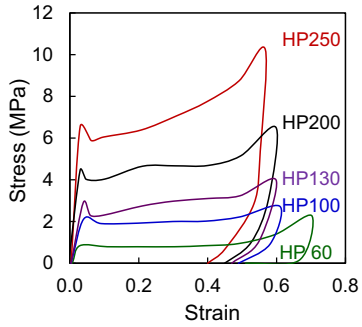


**Fig. 5.** Stress–strain curves for the DIAB Divinycell HP foam cores studied [24].

### 4.1. Modeling of water–structure interaction

The model consists of a Lagrangian domain for the solids and an Eulerian domain for the water. In the Lagrangian domain, nodes are fixed within the material and nodal displacements track the material deformation. Since each Lagrangian element is always 100% within a single material, the material boundary coincides with element boundaries. In contrast, the Eulerian domain consists of nodes that are fixed in space and the material flows through the elements that do not experience deformation. Eulerian elements may also be partially or completely void, allowing material to flow into empty space, capturing a crucial aspect of fluid flow. Materials tracked by Eulerian elements can interact with Lagrangian elements through Eulerian–Lagrangian contact algorithms to allow fully coupled multi-physics simulations like fluid–structure interactions. Here, a coupled Eulerian–Lagrangian (CEL) framework is employed, as it allows the severe deformation in water and the FSI to be captured. In addition to simulating the blast wave propagation in the USLS, the Eulerian formulation also captures the exponentially decaying pressure waves and resulting cavitation at the fluid–structure interface.

The response of water is described by the Mie–Grüneisen equation of state

$$p = \frac{\rho_0 c_0^2 \eta}{(1-s\eta)^2}\left(1 - \frac{\Gamma_0 \eta}{2}\right) + \Gamma_0 \rho_0 E_m \tag{3}$$

where $p$ is pressure, $c_0$ is the speed of sound, $\rho_0$ is initial density, $E_m$ is internal energy per unit mass, $\Gamma_0$ is Grüneisen's gamma at a reference state, $s = dU_s/dU_p$ is the Hugoniot slope coefficient, $U_s$ is the shock wave velocity, and $U_p$ is particle velocity which is related to $U_s$ through a linear Hugoniot relation: $U_S = c_0 + sU_p$. The space

enclosed by the anvil shown in Fig. 2 is prescribed the properties of water while the space that is outside the anvil is kept as a "void", allowing water to flow into it as a result of high-pressure wave impinging on the target. This has the effect of instantaneously relieving the pressure in the water-chamber in a manner consistent with experimental observations.

### 4.2. Constitutive and damage models for PVC foams

Constitutive models for foams often rely on homogenized continuum descriptions of the cellular materials [28,29]. The PVC foam core used in the experiments is DIAB Divinycell HP [23] with densities of 60, 100, 130, 200 and 250 kg/m$^3$. The Deshpande and Fleck crushable foam plasticity model [26] is used to describe the constitutive behavior of the PVC foams. The yield surface for volumetric hardening is defined as

$$F=\sqrt{q^2+\alpha^2(p-p_0)^2}-B=0 \tag{4}$$

where $p$ is the pressure, $q$ is the von Mises stress, $\alpha=B/A$ is the shape factor of the yield ellipse that defines the relative magnitude of the axes. The shape factor is specified by

$$\alpha=3k/\sqrt{(3k_t+k)(3-k)}, \text{ where } k=\sigma_c^0/p_c^0 \text{ and } k_t=p_t/p_c^0, \tag{5}$$

where $\sigma_c^0$ is the initial yield stress in uniaxial compression, $p_c^0$ is the initial yield stress in hydrostatic compression and $p_t$ is the yield strength in hydrostatic tension. Material parameters for the PVC foams are provided by the manufacturer [23]. Experiments performed show that fracture and fragmentation are significant damage mechanisms in composite sandwich structures subjected to underwater impulsive loads. A phenomenological damage criterion proposed by Hooputra et al. [27] is implemented to predict the onset of rupture due to strain localization and to capture the subsequent fragmentation of the core material. The damage model assumes that the equivalent plastic strain at the onset of damage ($\bar{\varepsilon}_D^{pl}$) is a function of stress triaxiality and equivalent plastic strain rate, i.e. $\bar{\varepsilon}_D^{pl}=\bar{\varepsilon}_D^{pl}(\eta,\dot{\bar{\varepsilon}}^{pl})$, where $\eta=-p/q$ is the stress triaxiality, $-p$ is the hydrostatic stress, $q$ is the von Mises equivalent stress and $\dot{\bar{\varepsilon}}_D^{pl}$ is the equivalent plastic strain rate. The criterion for damage initiation is met when $\omega_D=\int d\bar{\varepsilon}^{pl}/\bar{\varepsilon}_D^{pl}(\gamma,\dot{\bar{\varepsilon}}^{pl})=1$, where $\omega_D$ is a state variable that increases monotonically with plastic deformation. At each increment during the analysis, the incremental increase in $\omega_D$ is computed as $\Delta\omega_D=\Delta\bar{\varepsilon}^{pl}/\bar{\varepsilon}_D^{pl}(\eta,\dot{\bar{\varepsilon}}^{pl})\geq 0$. The evolution of damage is based on fracture energy per unit area dissipated during the damage process. The data for fracture toughness is obtained from experiments carried out by Poapongsakorn and Carlsson [30].

### 4.3. Water-tank, projectile, piston, platens and supports

The water-tank and supports are made of stainless steel, and the piston, projectile and platens are made of aluminum. A Lagrangian formulation is adopted for these components with linear elastic constitutive behavior.

### 4.4. Alleviating mesh dependence in numerical analyses

Failure is predicted when the damage operator in the respective case reaches unity. Once this rupture criterion is satisfied, the strengths of failed elements are set to zero. However, the predictions of damage and structural response based on such failure criteria are inherently mesh-size dependent as shown by Needleman and Tvergaard [31] and Gullerud et al. [32]. When the stress–strain diagram exhibits a negative slope, the strain-softening damage tends to localize in a zone that is governed by element size. Since the damage dissipation per unit volume is finite, the vanishing damage zone causes the structure to fail at zero energy dissipation. In the current computational approach, the mesh size selection must ensure satisfactory strain resolution, realistic energy dissipation and must qualitatively reflect the experimentally observed deformation modes.

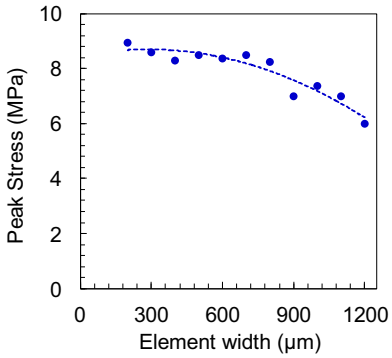


**Fig. 6.** Peak stress in the compressed foam as a function of element size for an impulsively loaded HP60 sandwich plate.

To counteract this spurious mesh dependence associated with material softening, a characteristic element length $L_E$ is introduced in ABAQUS. For 3-D elements, $L_E$ is the cube-root of element volume. Following damage initiation, an equivalent displacement $\delta$ is introduced such that $\delta=L_E\cdot\varepsilon$ and evolves according to $\dot{\delta}=L_E\cdot\dot{\varepsilon}$ until it reaches a critical value. Although mesh refinement is essential for adequate strain resolution, excessive mesh refinement has the adverse effect of yielding anomalously low energy dissipation. As shown in Fig. 6, the numerical solution reaches convergence for a mesh width of $w=500\,\mu\text{m}$ for an incident impulse of $\bar{I}=0.25$ for the HP60 core (which experiences the highest compressive strain). Consequently, the mesh width selected for this calculation is $w=500\,\mu\text{m}$, which is sufficient for numerical convergence (in both, bulk and cohesive elements) but still provides a reasonable approximation of energy dissipated in the process.

## 5. Loading–structure–performance maps

To fully utilize the potential of sandwich structures, one consideration is to maximize the performance for a give load setting while minimizing the mass. The weight-efficient designs of blast-resistant structures are determined by a number of factors, such as the expected incident load, facesheet and core materials, structural dimensions, geometry and interfacial effects. To quantify the effect of these factors on deformation response, structural indices are developed. Non-dimensional variables are used for quantitative evaluation of the compressive response of the PVC foams and the structural response of composite panels as functions of loading and structural attributes. The performance attribute of interest here is the compressive strain $\varepsilon$, transmitted impulse $I_B$ (kPa·s) and normalized transmitted impulse $\bar{I}_B$, the material attribute of interest is the normalized relative density $\bar{\rho}$ and the load is the normalized incident impulse $\bar{I}$. These parameters are varied independently of each other and the performance of each structure is quantified using these parameters. Based on the experiments and numerical simulations reported here, loading–structure–performance maps are developed. These maps can be used to inform structural design with the understanding that they should only be used for the specified material, structural parameter ranges and loading conditions specified.

## 6. Results and discussion

### 6.1. Experimental results and numerical validation

The experimental results are used to calibrate the computational model and evaluate response over a wide range of loading and structural attributes. Fig. 7 shows high-speed photographs and corresponding computational contour plots for strain in the HP60 foam subjected to loading with $\bar{I} = 0.25$. After the onset of loading, the core undergoes large compressive deformation rather uniformly throughout the thickness. After 750 μs, strain localization occurs near the frontface and backface. At 1000 μs, the core compression is complete and strain localization severe throughout the specimen. Fig. 8 shows the compressive response of the HP100 foam subjected to loading with $\bar{I} = 0.25$. In a manner quite similar to the case for the HP60 foam, the strain in the HP100 core is distributed relatively uniformly throughout the thickness and strain localization occurs at multiple locations. The overall compressive strain is lower than that in the HP60 foam and sites of localized straining coalesce into bands. For both the HP60 and HP100 core materials, the bands are not limited to either the frontface or the backface. Rather, they emanate from the frontface and propagate gradually through the thickness, spanning the whole cross-section.

Figs. 9 and 10 show high-speed photographs and corresponding calculated strain fields in HP200 and HP250 foam subjected to loading with $\bar{I} = 0.25$, respectively. In both specimens, the strains and resulting strain localization are concentrated at the base of the specimen near the distal face, precipitating inefficient impulse absorption and leading to large impulse transfer through the foam. The experiments and simulations show reasonable agreement in terms of the rate and extent of compression. Additionally, the simulations reveal characteristics of strain localization and deformation response that are difficult to obtain from experiments, thereby adding valuable insight into the response of each sandwich core. However, larger permanent compressions of the foam cores are observed in the experiments than in the calculations.

### 6.2. Deformation in the core

Fig. 11(a–d) shows the time histories of the corresponding compressive strain measured from high-speed digital images for all foams analyzed. For the HP60, HP100 and HP130 foams, rapid compression of the sample occurs immediately after the onset of loading, resulting in water leaking from the water tank of the USLS. As the density of the foam increases, both the rate and extent of core compression decrease significantly. Specifically, the HP200 and HP250 cores exhibit negligible compression and essentially behave like monolithic plates, indicating that there is no apparent advantage in using these foam materials in applications in which energy absorbency or compliance are desired. Instead, these foams may be desirable for applications that require high stiffness.

As the loading intensity increases, both the rate and extent of core compression increase substantially. For the highest load intensity considered, i.e. $\bar{I} = 0.25$, the HP60 core experiences maximum compression while the HP100 and HP130 cores show compressions that are 70% and 40% of that observed for HP60, respectively.

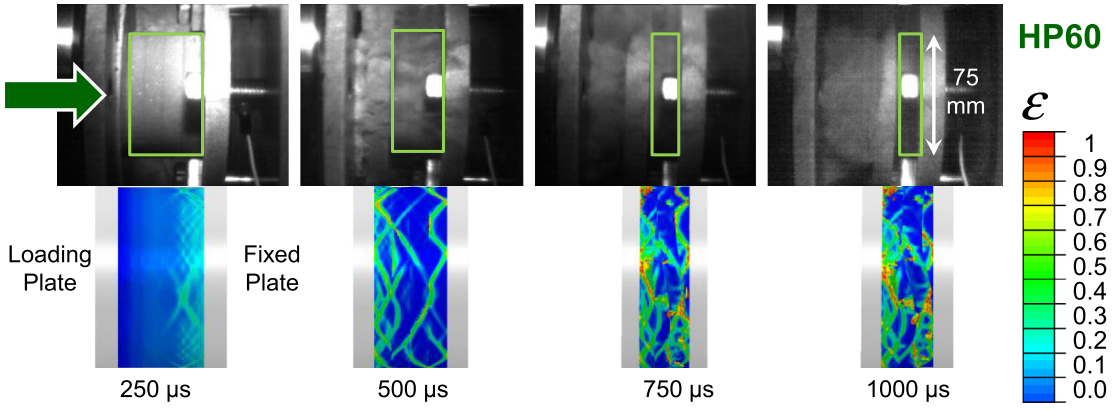


**Fig. 7.** A comparison of experimentally measured and numerically calculated strain fields at different times for a sandwich structure with the HP60 core subjected to $\bar{I} = 0.25$.

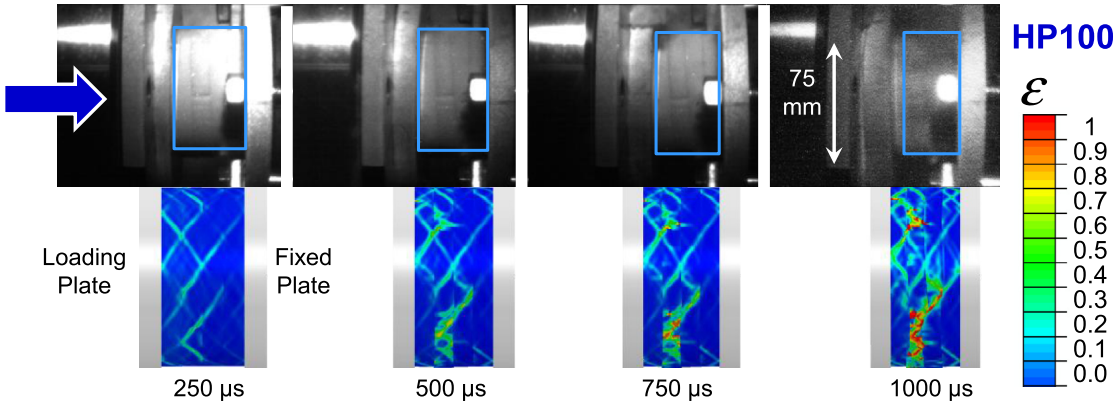


**Fig. 8.** A comparison of experimentally measured and numerically calculated strain fields at different times for a sandwich structure with the HP100 core subjected to $\bar{I} = 0.25$.

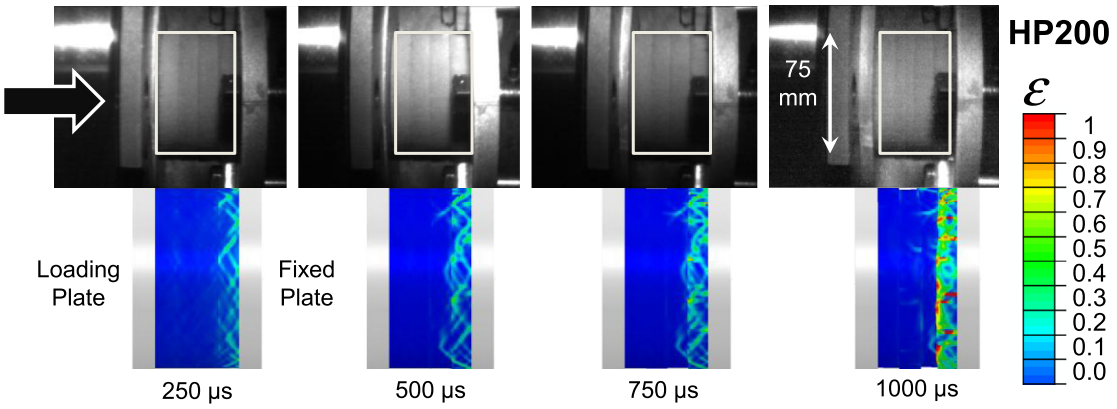


**Fig. 9.** A comparison of experimentally measured and numerically calculated strain fields at different times for a sandwich structure with the HP200 core subjected to $\bar{I} = 0.25$.

The compressive strains in the HP200 and HP250 cores are 30% and 10% of that observed in the HP60 core, respectively. Fig. 12 shows the loading–structure–performance map of compressive strain $(\varepsilon)$ as a function of the incident impulse $(\bar{I})$ and relative density $(\bar{\rho})$. At all impulse magnitudes, foams with the lowest relative density experience the highest compressive strain. The compressive strain increases as the relative density increases and as the impulse magnitude increases. The HP250 and HP200 cores exhibit significantly higher resistance to crushing compared with the HP60, HP100 and HP130 foam cores. As the core density increases, the maximum core compression increases monotonically up to $\bar{\rho} = 0.05$. With increasing core density, the maximum core compressive strain plateaus at $\bar{I} = 0.12$.

### 6.3. Impulse transmission through the core

The composite structure that transmits the least impulse at the lowest rate is most desirable. Fig. 13(a–d) shows the reaction forces measured by the force transducer for all cores and the input impulse magnitudes. At the higher load intensities $(\bar{I} = 0.15 \text{ and } 0.25)$, the crushing and collapse of the core material result in high intensities of transmitted impulse. Core indentation is particularly harmful for sandwich structures as it causes instabilities in the frontface which lead to buckling and shear failure as well as increased impulse transmission. Fig. 14(a–d) shows the corresponding transmitted impulse histories for all cores and input impulse magnitudes. Lower transmitted impulse indicates better blast mitigation capability. The results show that core density and load intensity both strongly affect impulse transmission. Structures with low density cores consistently outperform structures with high density cores. The effects of core characteristics can be compounded by loading rate.

A comparison of Figs. 11 and 14 reveals that the rate and extent of core compression correlate with the transmitted impulse, with low density cores undergoing high compressive strains and providing higher blast mitigation than high density cores. These trends are observed at all loading intensities, with the low density cores (HP60, HP100 and HP130) transmitting significantly lower impulses than the high density cores (HP200 and HP250). This trend is consistent with deformation fields implied in the contour plots for strain shown earlier. Overall, the uniform distribution of strain and high strain levels in low density cores yield low impulse transmission; and non-uniform distribution of strain and lower strain levels in high density cores lead to high impulse transmission. Although the total momentum imparted to the sandwich plates is lower for low density cores, the kinetic energy acquired by the frontface is higher in such cases. This results in greater core compression which is detrimental to residual bending stiffness and strength. Since core compression and impulse transmission can pose opposing requirements on structural parameters, an optimum design must balance the competing requirements. Such a design may be different for different load conditions and intensities.

Fig. 15(a) shows the loading–structure–performance map of transmitted impulse $(I_B)$ as a function of incident impulse $(\bar{I})$ and relative density $(\bar{\rho})$. At all impulse magnitudes, foams with the lowest

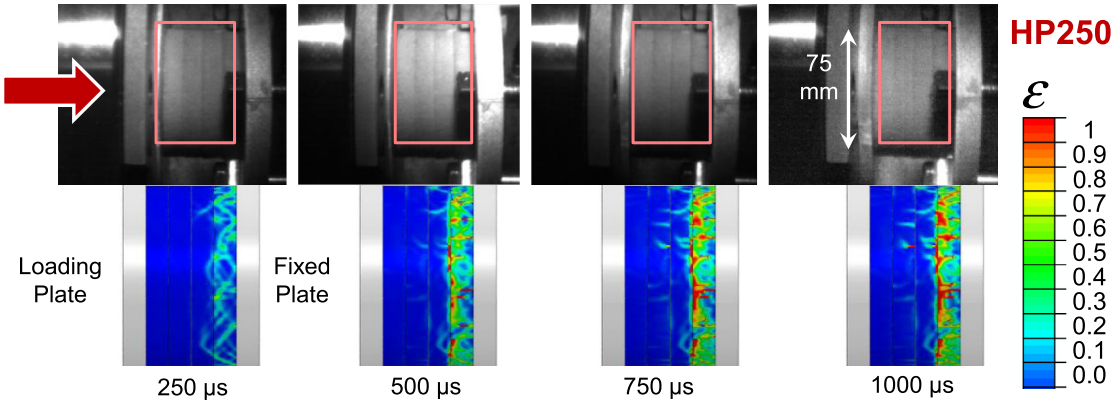


**Fig. 10.** A comparison of experimentally measured and numerically calculated strain fields at different times for a sandwich structure with the HP250 core subjected to $\bar{I} = 0.25$.

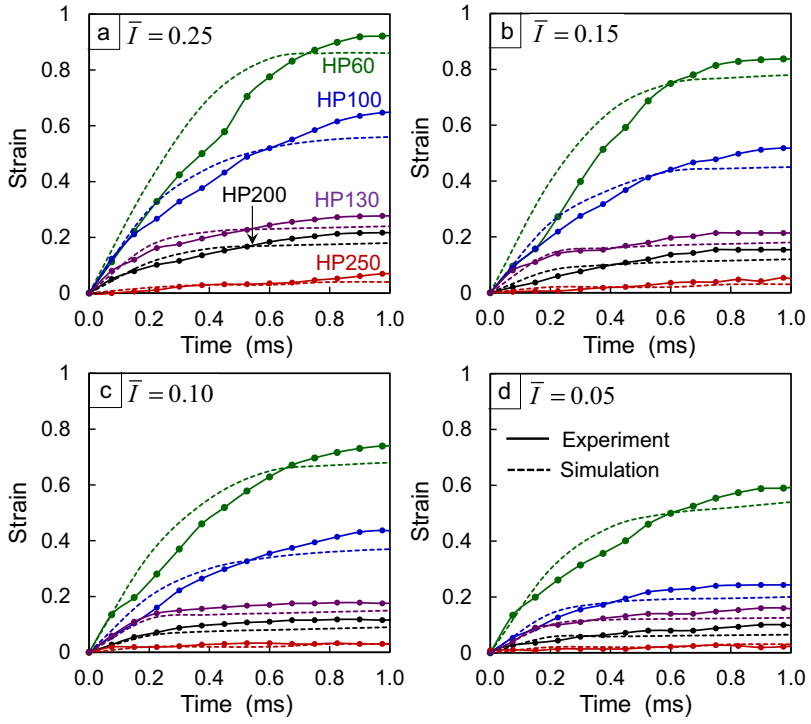


**Fig. 11.** Experimentally measured and numerically calculated strain histories for cases with the HP60, HP100, HP130, HP200 and HP250 cores subjected to loading at different intensities.

relative density transmit the least impulses. The transmitted impulses are strongly dependent on relative density and increase with increasing relative density as well as impulse magnitudes. HP60, HP100 and HP130 foam cores exhibit significantly higher blast mitigation capacity in comparison to HP200 and HP250 foam cores. Fig. 15(b) shows the normalized transmitted impulse $(\bar{I}_B)$ for all 20 foam core specimens as a function of the incident impulse $(\bar{I})$ and relative density $(\bar{\rho})$. The variation of $\bar{I}_B$ with $\bar{I}$ and $\bar{\rho}$ is quite different from those observed for $I_B$. The transmitted impulse as a fraction of incident impulse seems to be only weakly influenced by the incident impulse magnitude but very strongly influenced by the core density. This highlights the fact that in structural design of sandwich composites, the selection of material for the sandwich core is of utmost importance.

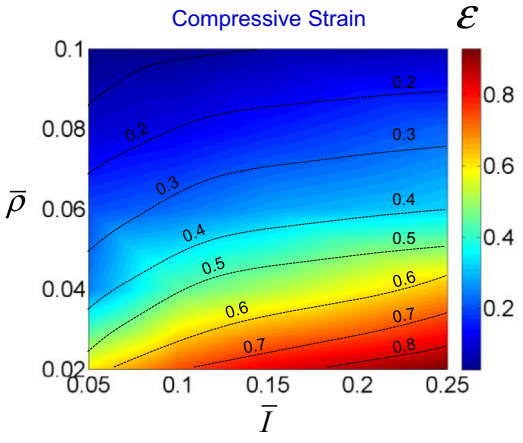


**Fig. 12.** Loading–structure–performance map showing compressive strain in the sandwich core as a function of incident impulsive load intensity $\bar{I}$ and normalized density $\bar{\rho}$.

It should be noted that although low density cores transmit the least impulses, they also undergo high compressive strains and thereby render the structure more susceptible to collapse. The experiments and calculations are in good agreement, indicating that the homogenized Deshpande and Fleck constitutive model [26] in combination with the Hooputra et al. damage criterion [27] provides a reasonably accurate representation of the deformation in the sandwich core. It should be noted that the Deshpande and Fleck constitutive model slightly overestimates the compliance of the foam core, leading to a higher initial rate of core compression and marginally greater transmitted impulses.

### 6.4. *Effect of face thickness on deformation and impulse transmission*

The effect of facesheet thickness is analyzed by systematically varying both the front and back facesheet thicknesses and by evaluating the response of each sandwich core. The facesheet thicknesses considered are 4, 6, 8 and 10 mm, giving $(\Delta T_f/T_c)$ and $(\Delta T_b/T_c)$ of 0.08, 0.12, 0.16 and 0.2, where $\Delta T_f$ and $\Delta T_b$ are the changes in front and back face thicknesses respectively. Fig. 16 shows a comparison of experimentally observed and calculated compressive response of the structure with the HP100 core with $(\Delta T_f/T_c) = 0.2$.

Strain localizes predominantly near the impulse face and near the distal face due to significant wave reverberations. It is instructive to note the differences between the responses of the HP100 core with $(\Delta T_f/T_c) = 0.2$ and with $(\Delta T_f/T_c) = 0$ shown in Fig. 8. For $(\Delta T_f/T_c) = 0$, the compressive strain is relatively uniform throughout the thickness. For $(\Delta T_f/T_c) = 0.2$, the compressive strain tends to localize near the facesheets. Fig. 17(a) shows the compressive strain and Fig. 17(b) shows the history of the corresponding transmitted impulse for structures with the HP100 core and different frontface thicknesses under loading with $\bar{I} = 0.25$.

As the frontface thickness increases, the strains increase and the transmitted impulse increases accordingly. Although thicker

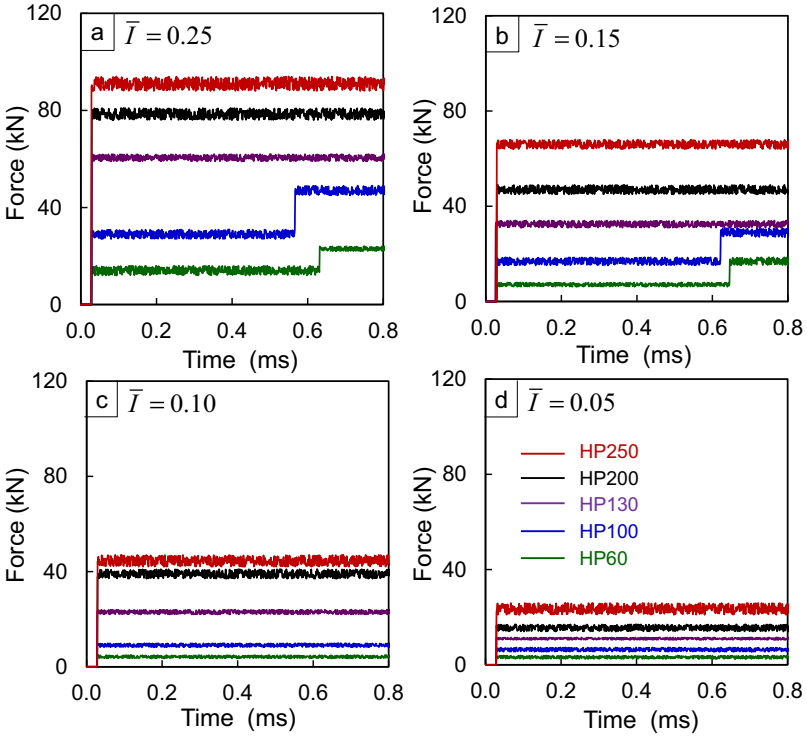


**Fig. 13.** Experimentally measured reaction force histories for sandwich plates subjected to impulsive loading of different intensities.

frontfaces tend to increase impulse transmission, sufficiently strong frontfaces are necessary for structural integrity. Therefore, sandwich structures must balance the strength and mass of the frontface and allowable core compression to control impulse transmission. Fig. 18 shows the effect of backface thickness on the transmitted impulse. As the backface thickness increases, the transmitted impulse decreases only slightly. Since the benefit is relatively negligible, the influence of backface thickness on structural response is not analyzed further. Fig. 19(a) shows the peak compressive strain ($\varepsilon$) and Fig. 19(b) shows the normalized transmitted impulse ($\bar{I}_B$) for all specimens as functions of frontface thickness ($\Delta T_f/T_c$) and relative density ($\bar{\rho}$) for $\bar{I} = 0.25$. The results reveal that both core

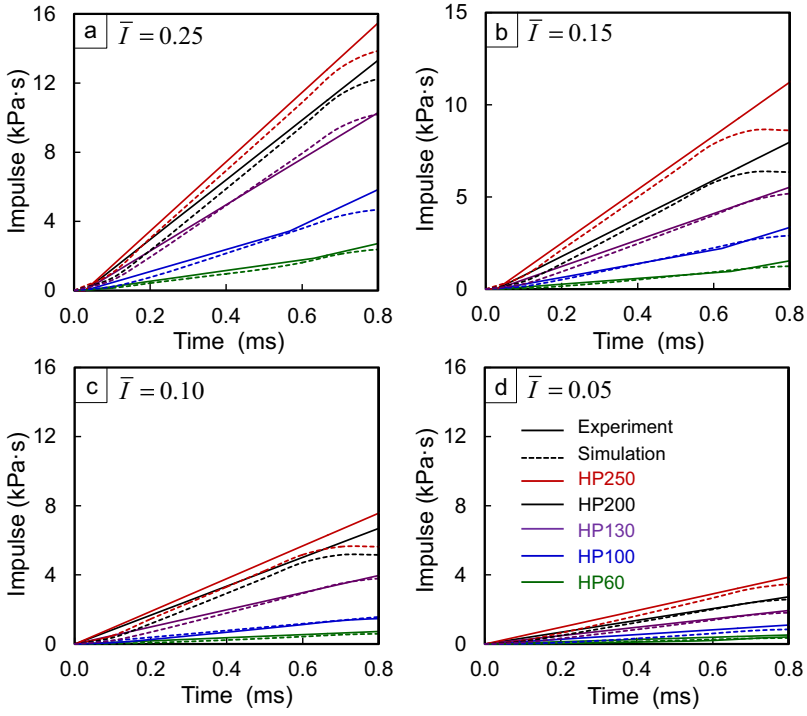


**Fig. 14.** Experimentally measured and numerically calculated transmitted impulse histories for Divinycell HP cores subjected to impulsive loading of different intensities.

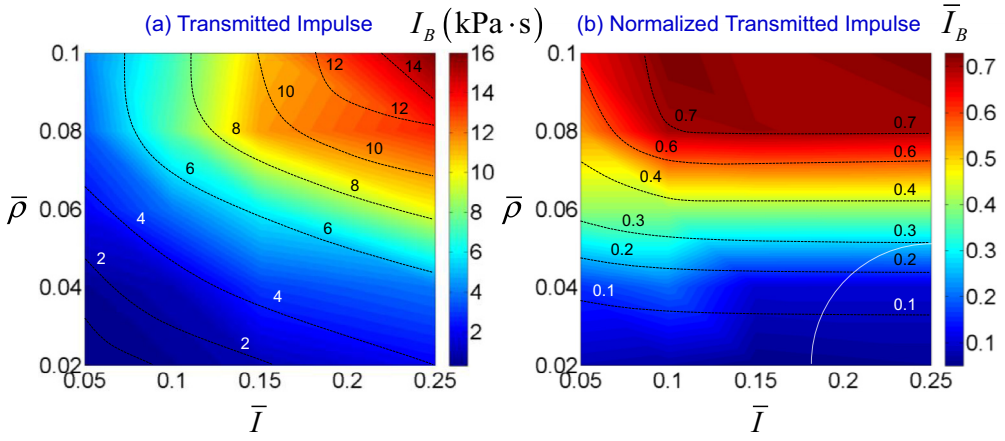


**Fig. 15.** Loading–structure–performance map showing (a) transmitted impulse $I_B$ (kPa·s) and (b) normalized transmitted impulse $\bar{I}_B$ as functions of incident impulsive load $\bar{I}$ and normalized density $\bar{\rho}$. The region encircled by the white dotted line denotes cores that collapsed under impulses exceeding $\bar{I} = 0.10$ as shown in Fig. 13.

compressive strain and normalized transmitted impulse increase with increasing frontface thickness. For a 10% increase in frontface mass, the core compressive strain increases by ~5% and transmitted impulse increases by ~10%. Overall, the core density has a strong influence on blast resistance and the frontface thickness.

### 6.5. Comparison with analytical model

A number of analytical models have been developed to extend Taylor's relation for an underwater impulse impinging on a free-standing plate [17]. These relations are generally based on a

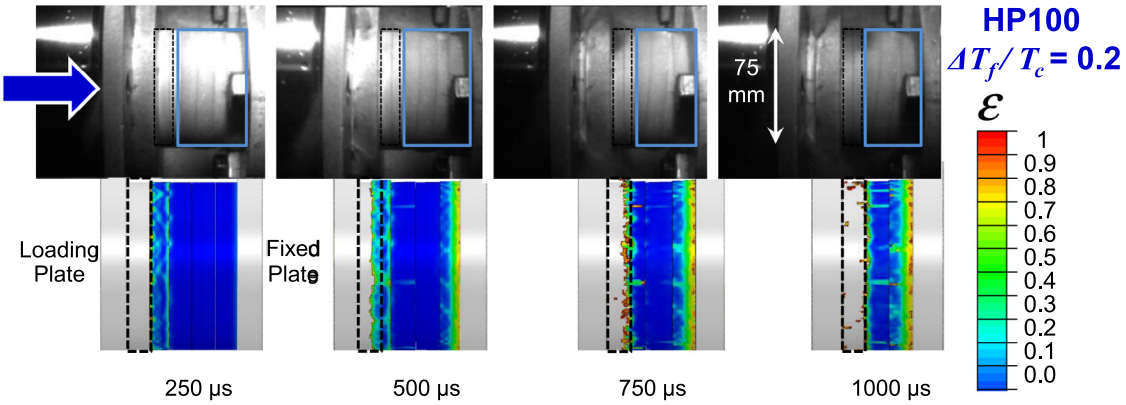


**Fig. 16.** A comparison of experimentally measured and numerically calculated strain fields at different times for a sandwich structure with the HP100 core ( $\bar{I} = 0.25$).

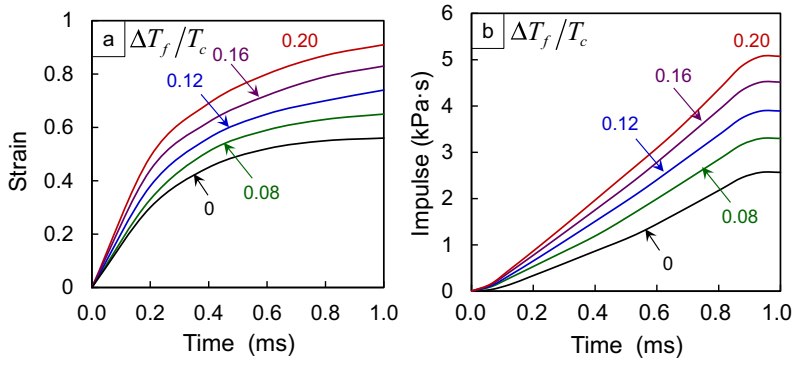


**Fig. 17.** Compressive strain and transmitted impulse histories for different $(\Delta T_f / T_c)$ values for the HP100 core subjected to $\bar{I} = 0.25$.

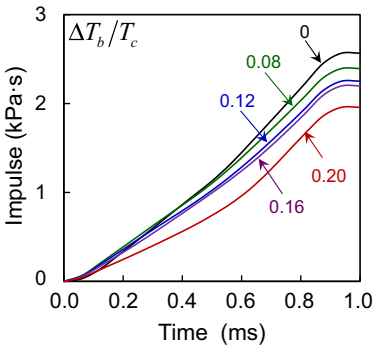


**Fig. 18.** Transmitted impulse histories for different ratios between backface thickness and core thickness $(\Delta T_b/T_c)$ for the HP100 core subjected to $\bar{I} = 0.25$.

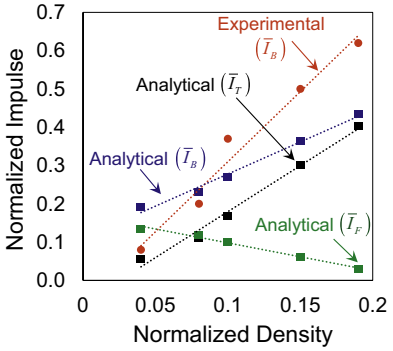


**Fig. 20.** A comparison of normalized transmitted impulse values obtained from experiments and calculated using Hutchinson and Xue's analytical approach [8].

simplified continuum description of the sandwich core. Fig. 20 shows a comparison between the predictions of Hutchinson and Xue's analyical model [8] and the experimental results obtained in the current study. The Hutchinson and Xue approach clearly delineates the benefit of sandwich plates over monolithic plates of equivalent mass and identifies minimum weight designs. This analytical model, based on a continuum description of the core, accurately predicts the transmitted impulses for low core densities, but significantly underestimates the transmitted impulses for high core densities.

## 7. Scaling and structural design

The underwater blast loading problem involves a wide range of length and time scales such as the spatial decay of the blast impulse, blast attenuation, pressure decay time, the size and geometry of the structure, and the area under impulsive loading relative to the total area of the structure. The characteristics of high intensity pressure pulses resulting from underwater blasts have been well established through large-scale experiments. In the analysis reported here, the underwater blast loading problem is simplified to delineate the performance of the sandwich core and provide a clear understanding of the role of core thickness, core density and facesheet thickness on blast response. The test specimen is designed such that the structure experiences one-dimensional, uniaxial compressive loading. This eliminates the complexities associated with large scale beam bending and facesheet stretching in blast loaded sandwich plates. The momentum transmitted into the sandwich plate is highly dependent on core strength and density. Denser cores $(\bar{\rho} > 0.06)$ better resist the motion of the frontface and lead to greater momentum transfer. At impulse intensities $\bar{I} > 0.15$, cores with $\bar{\rho} < 0.06$ undergo densification and collapse.

On the other hand, for $\bar{I} > 0.15$ and $\bar{\rho} > 0.06$, $\varepsilon$ is 0.2 and almost constant at all loading intensities. The momentum transmitted into the sandwich plates for $\Delta T_f/T_c < 0.1$ is substantially lower than that for $\Delta T_f/T_c > 0.15$. For the same core density, a 100% increase in facesheet thickness leads to a 25% and 50% increase in the core strain and in normalized transmitted impulse, respectively. For a given incident impulse, $\Delta T_f/T_c > 0.15$ results in more severe core compression because the impulse acquired by the frontface increases in proportion to mass.

A set of experiments and simulations is carried out to correlate the performance of the sandwich plates under uniaxial compression with the performance under bending of a blast loaded sandwich plate [33]. Fig. 21 shows a schematic illustration of the USLS with a simply-supported loading configuration. The sample size considered here is approximately one order of magnitude smaller than composite sections used in ships. The impulsive loads considered in this set of calculations have peak pressures of 40, 90, 140 and 175 MPa, which approximately correspond to 100 kg of TNT detonating at distances of 5.8, 2.83, 1.9 and 1.5 meters, respectively. These impulsive loads are of greater intensity than those analyzed using the Dynacomp setup. The facesheets are made of biaxial E-glass/vinylester composites and the core is PVC foam manufactured by

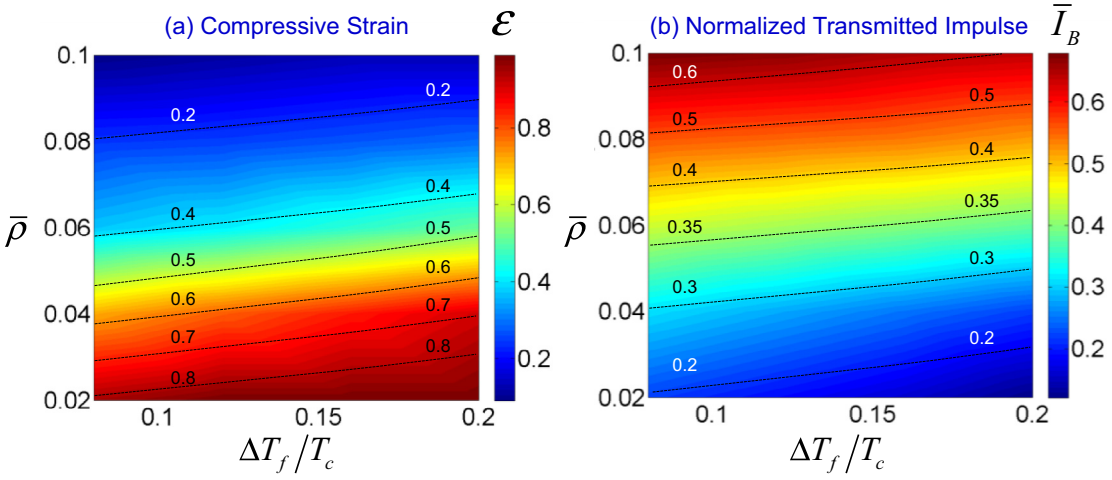


**Fig. 19.** Loading–structure–performance map showing compressive strain $\varepsilon$ and normalized transmitted impulse $\bar{I}_B$ as functions of $(\Delta T_f/T_c)$ and normalized density $\bar{\rho}$.

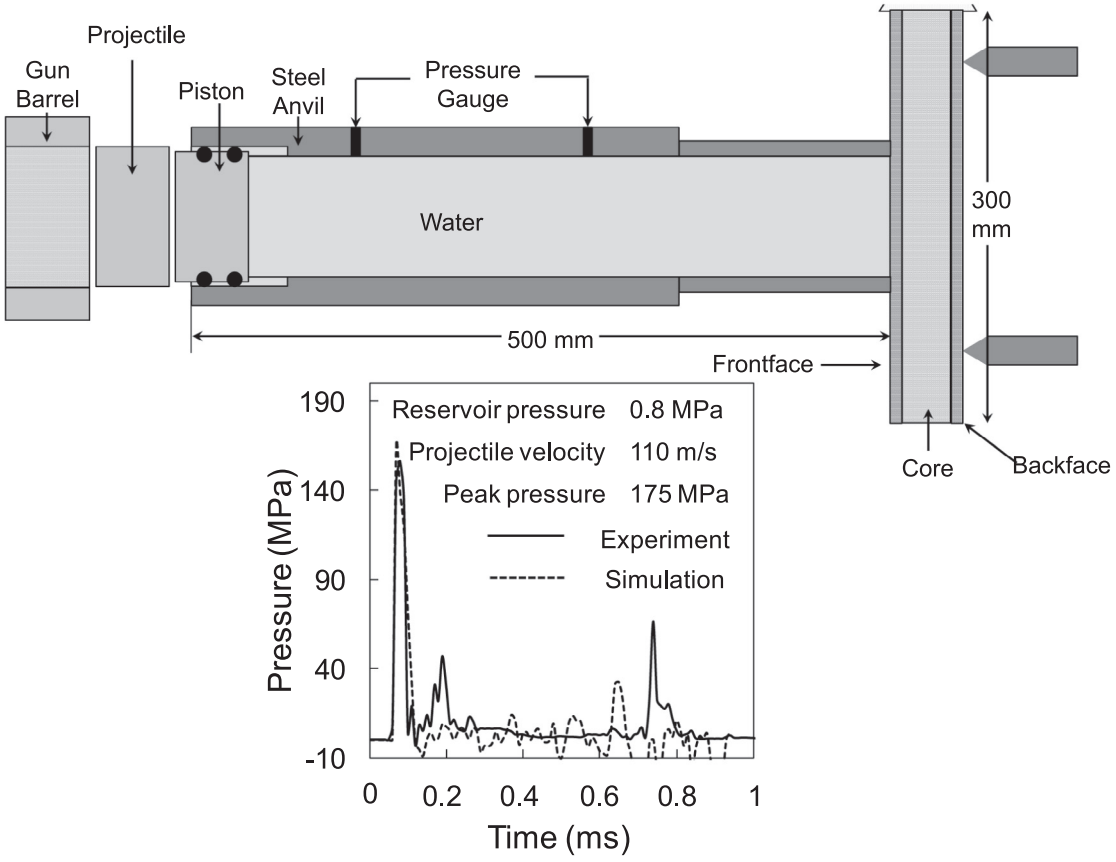


**Fig. 21.** A schematic illustration of the simply-supported air-backed loading configuration within underwater shock loading simulator (USLS).

DIAB Inc. [23]. Three PVC foam densities are analyzed: 60, 100 and 200 kg/m$^3$. The designs considered in this analysis have similar areal masses. To compare the effects of different core densities on response, a relative density $\bar{\rho}$ is defined such that $\bar{\rho} = \rho_{core}/\rho_{face}$.

Fig. 22 shows a sequence of high-speed photographs of the deformation in different composite structures subjected to $p_0 = 175\,\text{MPa}$, which is the highest load intensity considered in this analysis. Fig. 22(a) shows the response of monolithic composite plate. The deformation can be divided into two regimes: (1) flexural wave propagation toward the supports and (2) structural deflection. The flexural wave travels toward the supports in a very short time (~50 μs). Fig. 22(b) shows the response of a sandwich structure with HP200 core subjected to $p_0 = 175\,\text{MPa}$. The core fractures in a direction perpendicular to the planar wave and causes considerable core-face debonding in both the front and the back interfaces. Core compression is negligible and fragmentation is observed near the supports. Fig. 22(c) shows the behavior of a sandwich structure with HP100 core. The HP100 core fractures at an

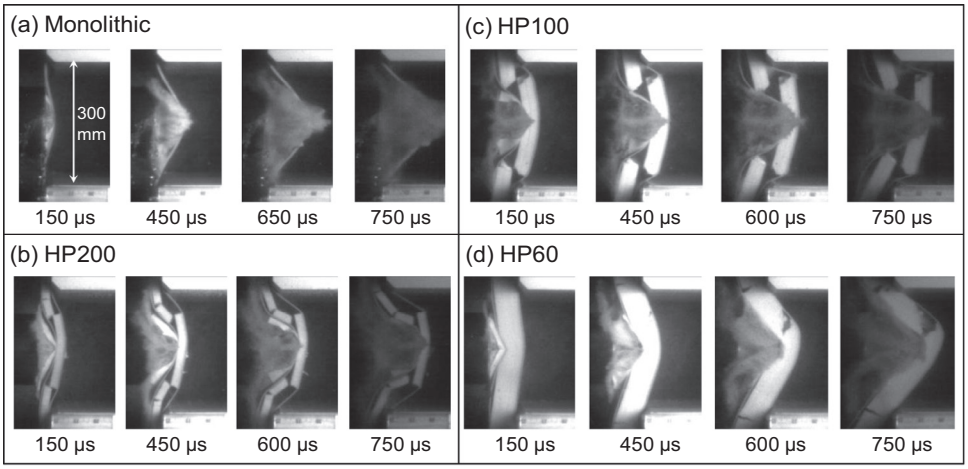


**Fig. 22.** Sequence of high-speed photographs showing the deformation in composite structures subjected to $p_0 = 175\,\text{MPa}$. The impulse imparted to the frontface causes it to move away at a velocity higher than the allowable dynamic crush rate of the core, resulting in large differential displacements which cause frontface fracture and core cracking, but relatively low core compression.

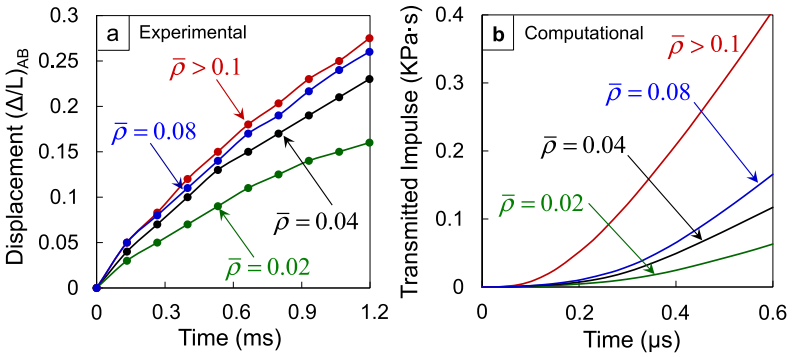


**Fig. 23.** (a) Experimentally measured midpoint displacements, and (b) computationally calculated measured transmitted impulses as functions of time for air-backed sandwich structures subjected to an impulse with.

inclined angle from the loading direction and simultaneously undergoes core compression and crushing. The response of a sandwich structure with an HP60 core is shown in Fig. 22(d). Core compression and frontface wrinkling are observed at $t = 150\,\mu s$. Core indentation occurs at $t = 300\,\mu s$ and the core starts to crack at $t = 450\,\mu s$. Damage and deformation in the sandwich structure with an HP60 core are significantly lower than those in the other structures. At high load intensities, it appears that the impulse imparted to the frontface causes it to move away at velocities higher than the allowable dynamic crush rate of the core, resulting in large differential displacements which cause frontface fracture and core cracking, but negligible core compression.

Fig. 23(a) shows the midpoint displacements as functions of time for the four different structures. The sandwich structures with HP200 and HP100 cores and the monolithic structures show relatively similar deformation histories reaching a $\Delta/L$ value of 0.25 at approximately the same rate. The sandwich structure with HP60 cores shows superior blast mitigation, deflecting at a lower rate and reaching a $\Delta/L$ value of 0.17, which is ~60% of that for the other sandwich structures. The results show that core density and load intensity profoundly affect both the rate and the extent of deformation in the composite structures. The study indicates that structure with low density cores consistently outperform structures with high density cores of equal mass. Lower core density and thicker cores correspond to reduction in velocity due to more significant core compression. Additionally, variations in geometric parameters have an effect on flexural rigidity and deformation. Since a fully 3D, dynamic computational framework is used in this analysis, structural effects beyond bending, as well as bending, are captured.

Minimizing the impulse transmitted to the internal components of marine vessels is of critical importance. The rate of impulse transmission and the magnitude of the transmitted impulse can provide valuable insight into the blast resistance and performance of composite structures. Clearly, the composite structure that transmits the least impulse at the lowest rate is most desirable. Fig. 23(b) shows the histories of impulses transmitted by air-backed structures subjected to incident impulsive loads of different magnitudes. For an incident impulse with $p_0 = 175\,\text{MPa}$, the sandwich structures with HP200, HP100 and HP60 cores transmit ~40%, 30% and 20% of the impulse transmitted by the monolithic composite, respectively. Correlating the rate of impulse transmission with the core characteristics in each case shows that, as the core density decreases and core thickness increases accordingly, the rate of impulse transmission decreases significantly.

Fig. 24 shows the normalized deflection $(\Delta/L)$ as a function of impulse $\bar{I}$ for structures with different normalized relative densities $\bar{\rho}$. A monotonically increasing trend of center deflections with increasing core density is seen and shows reasonable agreement with experiments. At all impulse magnitudes, structures with the lowest relative density experience the least deflections. The deflection increases with increasing relative density and impulse magnitude. The structure with the HP200 core performs only marginally better than monolithic structures. The HP100 and HP60 cores yield significantly higher blast resistances in comparison to the HP200 core and the monolithic composite. Fig. 25(a) shows the loading–structure–performance map of normalized deflection $(\Delta/L)_{AB}$ as a function of impulse $\bar{I}$ and relative density $\bar{\rho}$. As core density increases, the out-of-plane deflection of the sandwich plates increases dramatically. Fig. 25(b) shows the loading–structure–performance map of transmitted impulse for air-backed structures $(\bar{I}_B)$ as a function of normalized incident impulse $\bar{I}$ and normalized relative density s$\bar{\rho}$. At all impulse magnitudes, structures with the lowest relative density transmit the least impulse. The transmitted impulse increases with increasing relative density as well as impulse magnitude. HP200 cores perform better than monolithic structures while HP100 and HP60 cores exhibit significantly higher blast mitigation in comparison to HP200 core and the monolithic composite. Thus, low density cores lead to lower values of deflection as well as lower transmitted impulse at all impulse intensities.

The loading–structure–performance maps for uniaxial compressive loading (Figs. 12 and 15) are compared with those for the simply-supported bend loading configuration (Fig. 25) to gain insight into the role of core density on bending and failure. Higher core densities $(0.06 < \bar{\rho} < 0.1)$ limit core crushing, enable higher energy absorption and help maintain the bending strength of a sandwich plate, but result in significantly more momentum being imparted

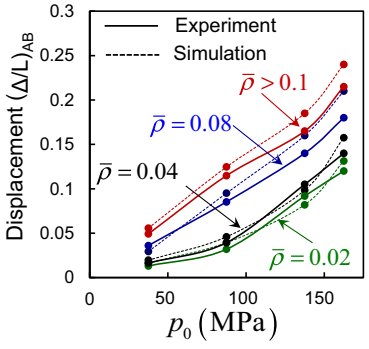


**Fig. 24.** Comparison of experimentally measured and numerically calculated mid-plane deflections at 1000 μs in air-backed structures as functions of normalized incident impulse $p_0$ for different normalized core densities. The results from experiments are in good agreement with those obtained from finite element simulations.

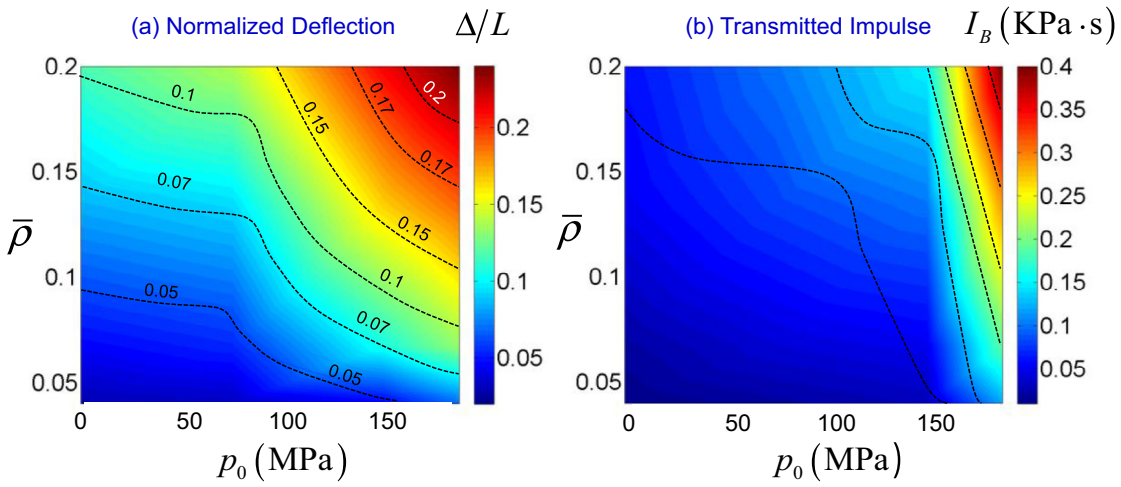


**Fig. 25.** Loading–structure–performance maps for simply-supported sandwich plates showing (a) deflection and (b) transmitted impulse as functions of peak pressure $p_0$ and normalized density $\bar{\rho}$.

to the structure. This leads to more severe core damage and out-of-plane deflection. Conversely, lower density cores $(0.01 < \bar{\rho} < 0.06)$ are susceptible to collapse under high intensity loads which can have adverse effects on survivability and residual bending strength. The trade-off between core compression and impulse transmission needs to be considered depending on application. In marine structures supported by stiffeners with water on the impulse side and air on the downstream side, the core has to provide load spreading and impulse absorption capabilities. Since an air-backed sandwich structure is free to deform in the out-of-plane direction, low density cores with $0.01 < \bar{\rho} < 0.06$ can satisfy both requirements [12,34,35].

Performance in water-backed conditions is important for the design of parts of ship structures like turbine blades, hull and keel. Water-backed conditions also prevail in underwater pipelines and ducts. In these cases, damage is localized and the structure is relatively undamaged in regions that are away from the loading area. Tensile loads and fracture in both faces are negligible due to the lack of overall deflection and bending, but the cores undergo severe compression [12,34,35]. Consequently, higher core densities are essential in order to maintain structural integrity in case of a blast event. Since minimizing core compression is essential in water-backed conditions, core densities with $0.06 < \bar{\rho} < 0.1$ are most optimal because data in Fig. 13(a–d) for $0.01 < \bar{\rho} < 0.06$ suggest that structures are susceptible to collapse under high intensity loads.

## 8. Concluding remarks

The conclusions of this study relating to the load-carrying and blast mitigation capacities of sandwich plates with polymeric foam cores are as follows:

(1) The compressive strain experienced by and the impulse transmitted by the sandwich core pose opposing requirements on structural design. Low density cores experience high compressive strains while transmitting lower impulses. On the other hand, high density cores behave like monolithic plates and transmit large fractions of the incident impulse. Although low density cores transmit significantly lower impulses, it should be noted that the kinetic energy acquired by frontfaces in low density cores is much higher, leading to severe core compression. This increased core compression is detrimental to bending stiffness and strength. Structural design must balance the competing requirements.

(2) Experiments and simulations are in reasonable agreement in terms of the extent of core compression and impulse transmission. Over the range of impulses and structural configurations considered, the finite element predictions are within 10% of the experimental data. The homogenized, crushable foam constitutive model employed provides accurate tracking of the early stage response of the core material. However, the model slightly overestimates the compliance of the core, leading to an increase in core compressive strain and a decrease in the transmitted impulses in comparison to experiments. The numerical calculations have provided an in-depth understanding of the temporal and spatial evolution of deformation modes in the core material.

(3) Cores with different densities show significantly different deformation behaviors. Low density cores like HP60, HP100 and HP130 $(0.01 < \bar{\rho} < 0.06)$ experience rather uniform straining throughout their thickness and provide high impulse mitigation capacity. High density cores such as HP200 and HP250 $(0.06 < \bar{\rho} < 0.1)$ experience strain localizations that occur primarily near the facesheets. Such non-uniform distribution of straining leads to high impulse transfer and severe damage in the core material.

(4) Loading–structure–performance maps derived from uniaxial compressive loading are compared to those obtained from the simply-supported bend loading configuration to offer insight into the role of core density on bending and failure of sandwich structures. The relative core density is found to be an important parameter determining the performance of sandwich structures in simply-supported conditions. Greater core compressibility minimizes both the deflection and impulse transmission in this configuration. Higher core densities $(0.06 < \bar{\rho} < 0.1)$ limit core crushing, enable higher energy absorption and help maintain the bending strength of a sandwich plate, but result in significantly more momentum being imparted to the structure. This leads to higher core damage and out-of-plane deflection. Conversely, lower density cores $(0.01 < \bar{\rho} < 0.06)$ are susceptible to collapse under high intensity loads which can have adverse effects on survivability and residual bending strength.

(5) The frontface and backface masses are varied independently and results indicate that the frontface mass has a significant influence on core compression and impulse transmission, while the backface mass has a negligible effect on

structural response. The momentum transmitted into the sandwich plates with $\Delta T_f/T_c < 0.1$ is substantially lower than that for $\Delta T_f/T_c > 0.15$. For the same core density, a 100% increase in facesheet thickness leads to a 25% and 50% increase in the core strain and normalized transmitted impulse, respectively. The greatest momentum transfer occurs in the case of monolithic plates of equivalent mass as sandwich plates. For a given incident impulse, $\Delta T_f/T_c > 0.15$ results in severe core compression and collapse because the impulse acquired by the frontface increases in proportion to mass.

In this combined experimental and numerical study, a parametric approach is employed to develop loading–structure–performance maps to quantify core compression, deflection and impulse transmission as a function of incident load (air-backed or water-backed conditions, load intensity), structural attributes, and loading configurations. The insight gained here provides guidelines for the design of structures for which response to water-based impulsive loading is an important consideration.

## Acknowledgements

Support by the Office of Naval Research through grant numbers N00014-09-1-0808 and N00014-09-1-0618 (program manager: Dr. Yapa D. S. Rajapakse) is gratefully acknowledged. Calculations are carried out on the Athena HPC cluster in the Dynamic Properties Research Laboratory at Georgia Tech. MZ also acknowledges beneficial interactions through the CAS/SAFEA International Partnership Program for Creative Research Teams.

## References

[1] Steeves CA, Fleck NA. Collapse mechanisms of sandwich beams with composite faces and a foam core, loaded in three-point bending. Part II: experimental investigation and numerical modelling. Int J Mech Sci 2004;46:585–608.
[2] Tagarielli VL, Deshpande VS, Fleck NA. The dynamic response of composite sandwich beams to transverse impact. Int J Solids Struct 2007;44:2442–57.
[3] Schubel PM, Luo JJ, Daniel IM. Impact and post impact behavior of composite sandwich panels. Compos Part A-Appl Sci Manuf 2007;38:1051–7.
[4] Nemes JA, Simmonds KE. Low-velocity impact response of foam-core sandwich composites. J Compos Mater 1992;26:500–19.
[5] Mines RAW, Worrall CM, Gibson AG. The static and impact behavior of polymer composite sandwich beams. Composites 1994;25:95–110.
[6] Abot IMDJL. Composite sandwich beams under low velocity impact. Proc AIAA Conf 2001.
[7] Schubel PM, Luo JJ, Daniel IM. Low velocity impact behavior of composite sandwich panels. Compos Part A-Appl Sci Manuf 2005;36:1389–96.
[8] Hutchinson JW, Xue ZY. Metal sandwich plates optimized for pressure impulses. Int J Mech Sci 2005;47:545–69.
[9] Liang YM, Spuskanyuk AV, Flores SE, Hayhurst DR, Hutchinson JW, McMeeking RM, et al. The response of metallic sandwich panels to water blast. J Appl Mech-Trans Asme 2007;74:81–99.
[10] Xue ZY, Hutchinson JW. Preliminary assessment of sandwich plates subject to blast loads. Int J Mech Sci 2003;45:687–705.
[11] Xue ZY, Hutchinson JW. A comparative study of impulse-resistant metal sandwich plates. Int J Impact Eng 2004;30:1283–305.
[12] Avachat S, Zhou M. Dynamic response of composite sandwich structures subjected to underwater impulsive loads: experiments and simulations conference. In: Ferreira AJM, editor. Proceedings of the 16th international conference on composite structures, ICCS-16. Porto: FEUP; 2011.
[13] Avachat S, Zhou M. Dynamic response of submerged composite sandwich structures to blast loading. In: Shukla A, editor. Proceedings of the IMPLAST 2010 – SEM fall conference. Providence, Rhode Island, USA: 2010. October 12–14 2010.
[14] Latourte F, Gregoire D, Zenkert D, Wei XD, Espinosa HD. Failure mechanisms in composite panels subjected to underwater impulsive loads. J Mech Phys Solids 2011;59:1623–46.
[15] Wei XD, Tran P, de Vaucorbeil A, Ramaswamy RB, Latourte F, Espinosa HD. Three-dimensional numerical modeling of composite panels subjected to underwater blast. J Mech Phys Solids 2013;61:1319–36.
[16] Swisdak MM. Explosion effects and properties: part II – explosion effects in water, Technical Report, Naval Surface Weapons Center, Dahlgren, Virginia, USA, 1978.
[17] Taylor GI. The pressure and impulse of submarine explosion waves on plates. The scientific papers of G I Taylor, vol. III. Cambridge: Cambridge University Press; 1941. p. 287–303.
[18] Arora H, Kelly M, Worley A, Del Linz P, Fergusson A, Hooper PA, et al. Compressive strength after blast of sandwich composite materials. Philos Trans R Soc A-Math Phys Eng Sci 2014;372.
[19] Taylor GI. The scientific papers of G I Taylor. Cambridge: Cambridge University Press; 1963.
[20] Kambouchev N, Radovitzky R, Noels L. Fluid-structure interaction effects in the dynamic response of free-standing plates to uniform shock loading. J Appl Mech-Trans Asme 2007;74:1042–5.
[21] Hutchinson JW. Energy and momentum transfer in air shocks. J Appl Mech-Trans Asme 2009;76.
[22] Avachat S, Zhou M. Effect of facesheet thickness on dynamic response of composite sandwich plates to underwater impulsive loading. Exp Mech 2011;52:83–93.
[23] S.D. DIAB Inc. DeSoto, Texas 75115, USA. <http://www.diabgroup.com/europe/literature/e_pdf_files/man_pdf/H_man.pdf>; 2011 [accessed 05.05.11].
[24] George T, Deshpande VS, Sharp K, Wadley HNG. Hybrid core carbon fiber composite sandwich panels: fabrication and mechanical response. Compos Struct 2014;108:696–710.
[25] Hibbit, Karlsson, Sorensen Inc. Abaqus/explicit user's manual, version 6.9, 2009.
[26] Deshpande VS, Fleck NA. Multi-axial yield behaviour of polymer foams. Acta Mater 2001;49:1859–66.
[27] Hooputra H, Gese H, Dell H, Werner H. A comprehensive failure model for crashworthiness simulation of aluminium extrusions. Int J Crashworthines 2004;9:449–63.
[28] Zhang J, Kikuchi N, Li V, Yee A, Nusholtz G. Constitutive modeling of polymeric foam material subjected to dynamic crash loading. Int J Impact Eng 1998;21:369–86.
[29] Deshpande VS, Fleck NA. Isotropic constitutive models for metallic foams. J Mech Phys Solids 2000;48:1253–83.
[30] Poapongsakorn P, Carlsson LA. Fracture toughness of closed-cell PVC foam: effects of loading configuration and cell size. Compos Struct 2013;102:1–8.
[31] Needleman A, Tvergaard V. Mesh effects in the analysis of dynamic ductile crack-growth. Eng Fract Mech 1994;47:75–91.
[32] Gullerud AS, Gao XS, Dodds RH, Haj-Ali R. Simulation of ductile crack growth using computational cells: numerical aspects. Eng Fract Mech 2000;66:65–92.
[33] Avachat S, Zhou M. High-speed digital imaging and computational modeling of dynamic failure in composite structures subjected to underwater impulsive loads. Int J Impact Eng 2015;77:147–65.
[34] Avachat S, Zhou M. Effect of core density on deformation and failure in sandwich composites subjected to underwater impulsive loads. Int J Multiphys 2012;6.
[35] Avachat S, Zhou M. Dynamic response of submerged composite sandwich structures to blast loading. In: Shukla A, editor. IMPLAST 2010 – SEM fall conference. Providence, Rhode Island, USA: Society for Experimental Mechanics, Inc.; 2010.